Electronic Supplementary Material (ESI) for Journal of Materials Chemistry A.

Supporting Information for

Small Sized Fe-Co Sulfide Nanoclusters Anchored on Carbon for Oxygen Evolution

Yuanjun Liu,[a] Xulan Xie,[b] Guoxing Zhu,[b,] Yu Mao,[c] Yinan Yu,[b] Suxiao Ju,[a] Xiaoping Shen[b,*] Huan Pang[d]*

[a]School of Environmental and Chemical Engineering, Jiangsu University of Science and Technology, Zhenjiang 202018, China

[b]School of Chemistry and Chemical Engineering, Jiangsu University, Zhenjiang 212013, China

E-mail: zhuguoxing@ujs.edu.cn; xiaopingshen@ujs.edu.cn

[c]School of Chemistry and Chemical Engineering, University of South China, Hengyang, 421001, China

[d]College of Chemistry and Chemical Engineering, Yangzhou University, Yangzhou, 225009, China

Details of Calculation Methods.

Because the obtained cobalt sulfide was comprised by Co_9S_8 with cubic crystal structure, a Co_9S_8 unit cell (cell formula: $Co_{36}S_{32}$, cubic Fm-3m, α = 9.923 Å) was employed in this calculation study. The (111) facet of Co_9S_8 was chosen as the model surface for the subsequent calculation (Figure SI-1). The Brillouin zone was sampled with a *k*-point mesh of 3 × 3 × 1 for Co_9S_8 (111) surface; and a vacuum layer of 12 Å was applied. Upper half of substrate layers and adsorbates are fully relaxed while the lower half of substrate layers are fixed. Bader analysis was carried out to evaluate the charges of each atoms in the system. Because the obtained cobalt sulfide was comprised by Co_9S_8 with cubic crystal structure, a Co_9S_8 unit cell (cell formula: $Co_{36}S_{32}$, cubic Fm-3m, α = 9.923 Å) was employed in this work (Figure SI-1a). The (111) facet of Co_9S_8 (with the lowest surface energy and has been observed experimentally to be preferentially exposed) was chosen as the model surface for the subsequent calculation (Figure SI-1b, c).[1, 2]

The cell formula of Co_9S_8 (111) facet is $Co_{18}S_{16}$; while the formula of $Fe_6Co_{12}S_{16}$ is selected as the model for *c*-$FeCo_2S_y$ product. Randomly selected 520 structures of the total 18564 possible $Fe_6Co_{12}S_{16}$ structures (18C6) were optimized. The energy distribution of the random 520 structures is shown in Figure SI-2. The result is close to a standard normal distribution. Thus, the randomly selected 520 structures can represent all of the 18564 different $Fe_6Co_{12}S_{16}$ structures. The most stable three $Fe_6Co_{12}S_{16}$ structures were chosen for the following calculations (Figure SI-14).

For the calculation of H_2O absorption energy on the surface, the convergence threshold was set as 10^{-5} eV in energy and 0.05 eV $Å^{-1}$ in force. The adsorption energy of X is defined as:

(1) $$E_{ad}^{X} = E(X/substrate) - E(substrate) - E(X)$$

where E(X/substrate), E(substrate), and E(X) are the energies of X adsorbed on the substrate, the substrate, and X in the gas phase, respectively. The more negative of

E_{ad}^{X} is, the more strongly the species binds with the substrate.

Calculation of the Gibbs free energies and theoretical overpotential based on a single-site mechanism

The thermodynamic potential for the oxidation of water to produce oxygen, $2H_2O \rightarrow O_2 + 4H^+ + 4e^-$, is 1.23 V at standard conditions. In our case the OER is operated in alkaline conditions. The elementary steps can be written as follows [3, 4]:

(2) $OH^- + * \rightarrow OH^* + e^-$

(3) $OH^* + OH^- \rightarrow O^* + H_2O + e^-$

(4) $O^* + OH^- \rightarrow OOH^* + e^-$

(5) $OOH^* + OH^- \rightarrow O_2 + H_2O + e^-$

where * denotes the active sites. The Gibbs free energy change for steps (2-5) can be expressed as:

(6) $\Delta G_1 = \Delta G_{OH} - eU + \Delta G_{H+}(pH)$

(7) $\Delta G_2 = \Delta G_O - \Delta G_{OH} - eU + \Delta G_{H^+}(pH)$

(8) $\Delta G_3 = \Delta G_{OOH} - \Delta G_O - eU + \Delta G_{H+}(pH)$

(9) $\Delta G_4 = 4.92 - \Delta G_{OOH} - eU + \Delta G_{H+}(pH)$

Where U is the potential measured against normal hydrogen electrode (NHE) at standard conditions. The free energy change of the protons relative to the above specified electrode at non-zero pH (in our cases, pH = 13.6) is represented by Nernst equation as:

(10) $\Delta G_{H+}(pH) = -k_B T \ln(10) \times pH$

The sum of ΔG_{1-4} is fixed to the negative of experimental Gibbs free energy that is involved for the formation of two water molecules (1.23 × 4 = 4.92 eV). The Gibbs free energy differences of these intermediates include zero-point energy (ZPE),

thermal energy and entropy derived from partition functions [5, 6]. The ZPE correction is given by:

(11) $$E_{ZPE} = \sum_i \frac{hv_i}{2}$$

where h is Plank's constant, v_i is vibration frequency calculated based on the harmonic oscillator approximation. The standard molar vibrational thermal energy contribution is calculated by:

(12) $$U_{vib} = RT \sum_i \frac{hv_i / k_B}{e^{hv_i/k_BT} - 1}$$

where R is the gas constant, k_B is Boltzmann's constant. The standard molar vibration entropy is calculated by using the following expression:

(13) $$S_{vib} = R \sum_i [\frac{hv_i / k_BT}{e^{hv_i/k_BT} - 1} - \ln(1 - e^{hv_i/k_BT})]$$

Therefore, the standard molar Gibbs free energies are obtained by:

(14) $$G = E_{total} + E_{ZPE} + U - TS$$

(15) $$\Delta G = \Delta E_{total} + \Delta(E_{ZPE} + U - TS)$$

where E_{total} refers to the total energy obtained from DFT calculation. The energy difference ΔE is calculated relative to H_2O and O_2:

(16) $$\Delta E_{OH} = E_{OH} - E_{Surface} - (E_{H2O} - 1/2\ E_{H2})$$

(17) $$\Delta E_{O} = E_{O} - E_{Surface} - (E_{H2O} - E_{H2})$$

(18) $$\Delta E_{OH} = E_{OOH} - E_{Surface} - (2*E_{H2O} - 3/2\ E_{H2})$$

After obtaining all ΔG via above equations, the theoretical overpotential is then readily defined as the value that the maximum of $\{\Delta G_1, \Delta G_2, \Delta G_3, \Delta G_4$ (divided by $e)\}$ minus 1.23 V.

Details for the derivation of the theoretical Tafel slope based on a two-site mechanism

Let us assume the following two-site mechanism:

(19) $*Fe + OH^- = *Fe\text{-}OH_{ads} + e^-$

(20) $*Co + OH^- = *Co\text{-}OH_{ads} + e^-$

(21) $*Fe\text{-}OH_{ads} + *Co\text{-}OH_{ads} \rightarrow *Fe\text{-}O_{ads}\text{-}*Co + H_2O$

(22) $*Fe\text{-}O_{ads}\text{-}*Co + OH^- = *Fe\text{-}OOH_{ads} + *Co + e^-$

(23) $*Fe\text{-}OOH_{ads} + OH^- = *Fe\text{-}O_{2\ ads} + H_2O + e^-$

(24) $*Fe\text{-}O_{2\ ads} = *Fe + O_2$

in which "*Fe" and "*Co" denote metal oxide/oxyhydroxide sites at the surface. In the case when step (21) represents the rate-determining step (RDS), the total rate of the reaction is given as:

(25) $j = 4 \times F \times k_3 \times \theta_{OH,\,Fe} \times \theta_{OH,\,Co}$

where k_i is the rate constant of step (i) in the forward (+) or backward (–) direction, θ is the fractional occupancy of the intermediates on surface Fe or Co sites. By applying a formal kinetic approach, the theoretical Tafel slope for this scenario was then calculated. Assuming that the steps preceding the RDS (steps 19 and 20) are in quasi-equilibrium at low overpotentials/current densities, we obtain the following equations:

(26) $$k_1\, c_{OH}\,(1-\theta_{OH,Fe})\,e^{\frac{(1-\beta)FE}{RT}} = k_{-1}\,\theta_{OH,Fe}\,e^{\frac{-\beta FE}{RT}}$$

(27) $$k_2\, c_{OH}\,(1-\theta_{OH,Co})\,e^{\frac{(1-\beta)FE}{RT}} = k_{-2}\,\theta_{OH,Co}\,e^{\frac{-\beta FE}{RT}}$$

in which c_{OH} is the concentration of OH^- ions, β_i is the symmetry factor (we can assume that $\beta_1 = \beta_2 = \beta_3 = \beta_4 = \beta = 0.5$), F is the Faraday constant, E is the potential, R is the universal gas constant, and T is the absolute temperature. Since θ is close to 0 at low overpotentials/current densities, it can be approximated that $(1 - \theta_{OH}) = 1$. In that case we obtain:

(28) $$\theta_{OH,Fe} = \frac{k_1}{k_{-1}} c_{OH} e^{\frac{FE}{RT}}$$

(29) $$\theta_{OH,Co} = \frac{k_2}{k_{-2}} c_{OH} e^{\frac{FE}{RT}}$$

Now, by replacing $\theta_{OH, Fe}$ and $\theta_{OH, Co}$ in the rate law of the total reaction (Eq. 25),

(30) $$j = 4 \times F \times k_3 \times \frac{k_1}{k_{-1}} \times \frac{k_2}{k_{-2}} \times c_{OH}^2 \times e^{\frac{2FE}{RT}}$$

For T = 298 K, the theoretical Tafel slope expected on *c*-$FeCo_xS_y$/carbon in the low current density range is:

(31) $$b = \frac{2.303RT}{2F} = 30 \text{ mV dec}^{-1}$$

This value is very close to the measured Tafel slope value of our obtained $FeCo_2S_y$/carbon product, 35 mV dec^{-1}. This result suggests that the step (21) that locates between the second and third electron transfer would be one possible RDS.

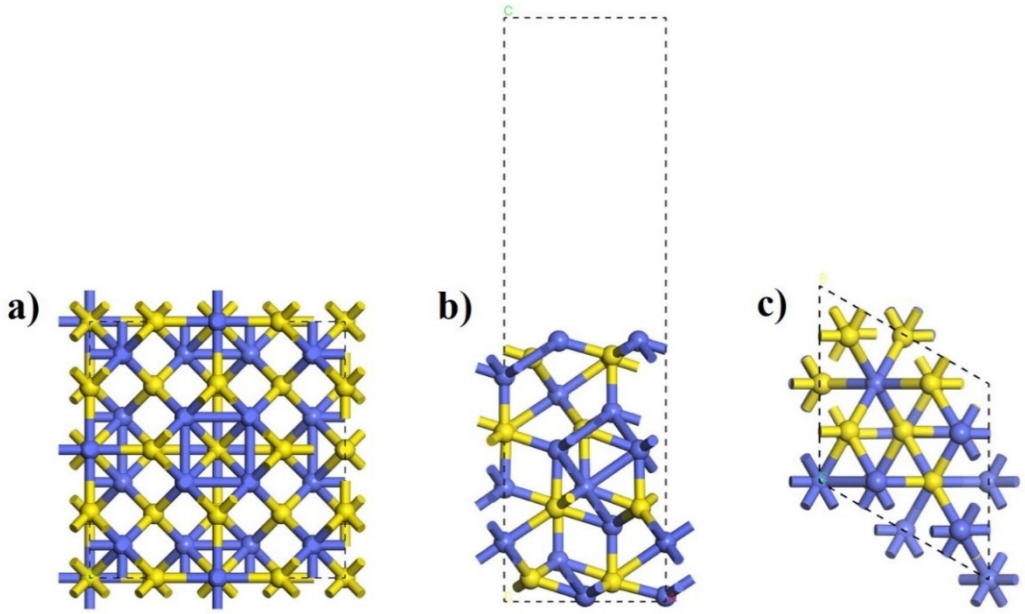

Figure SI-1. a) Crystal structure of Co_9S_8 and b, c) the side or top views of the Co_9S_8 (111) facet with the lowest surface energy.

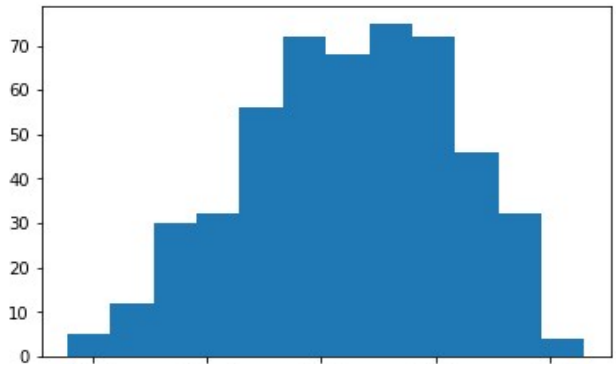

Figure SI-2. The energy distribution histogram of the 520 randomly selected $Fe_6Co_{12}S_{16}$ structures.

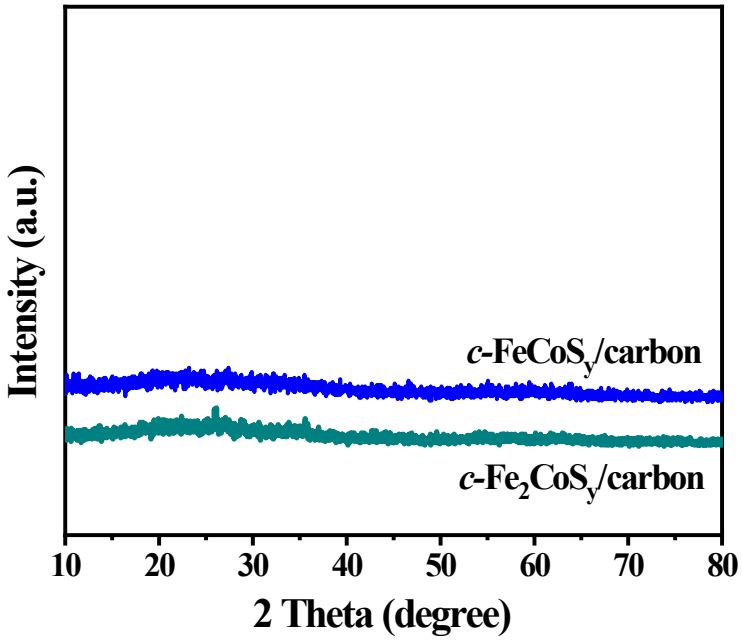

Figure SI-3. XRD patterns of *c*-$FeCoS_y$/carbon and *c*-Fe_2CoS_y/carbon.

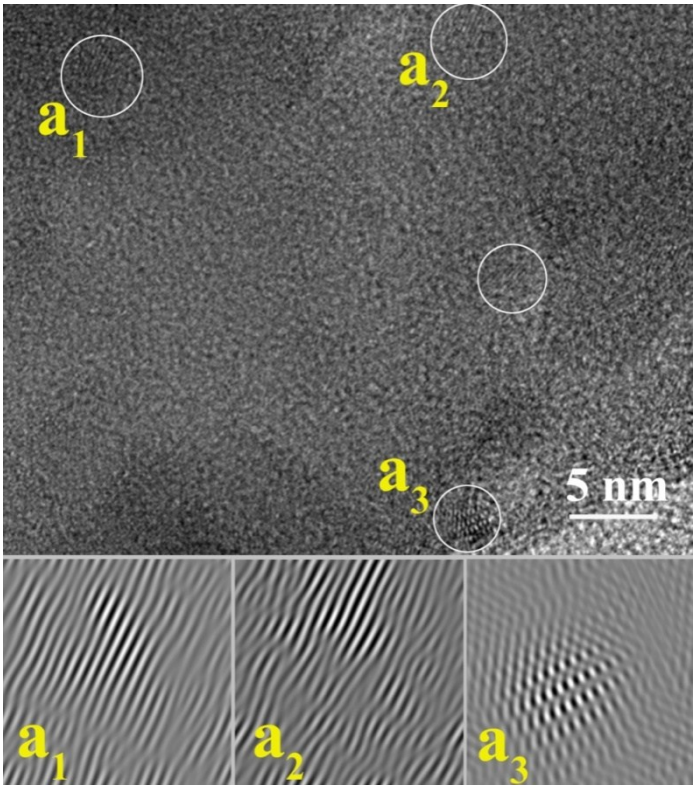

Figure SI-4. HRTEM image of the *c*-$FeCo_2S_y$/carbon product and the corresponding sharpen areas a_1-a_3).

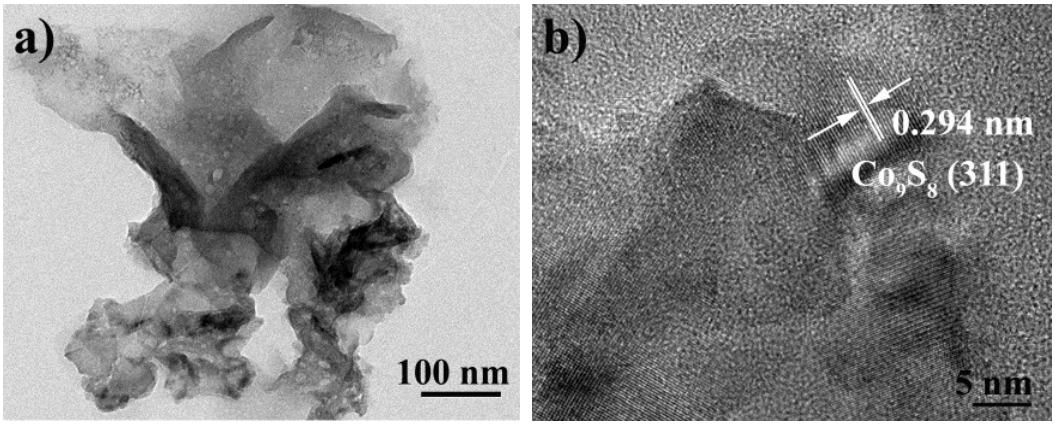

Figure SI-5. a) TEM and b) HRTEM images of CoS_y/carbon product.

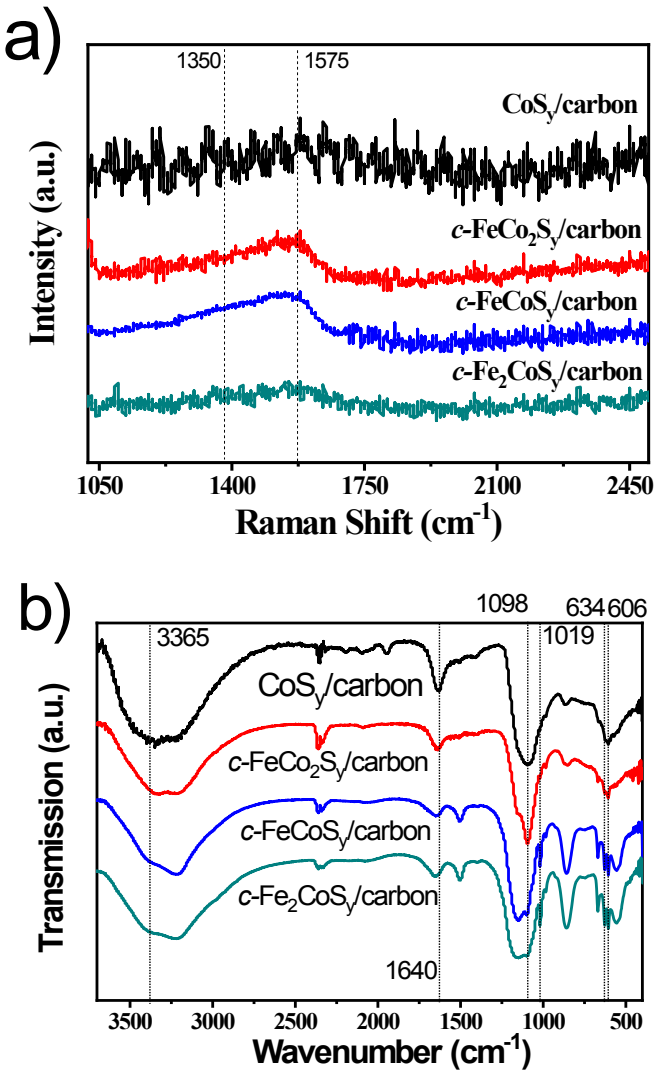

Figure SI-6. a) Raman spectra and b) FT-IR spectra of the obtained products.

In the spectrum, the peak centered at 2380 cm^{-1} is caused by asymmetrical stretching vibration of CO_2 that possibly comes from air. The peak at 880 cm^{-1} can be corresponded to the species of C-H in C=C-H (bending vibration). The relatively wide band at 1180 cm^{-1} indicates there are some C-O groups on the carbon materials (stretching vibration of C-O). In addition, the Fe-O species were also detected in the IR spectrum at wavenumber of 550 cm^{-1} for the Fe-rich products (*c*-$FeCoS_y$/carbon and c-Fe_2CoS_y/carbon), possibly due to the surface oxidation of sulfides in air.

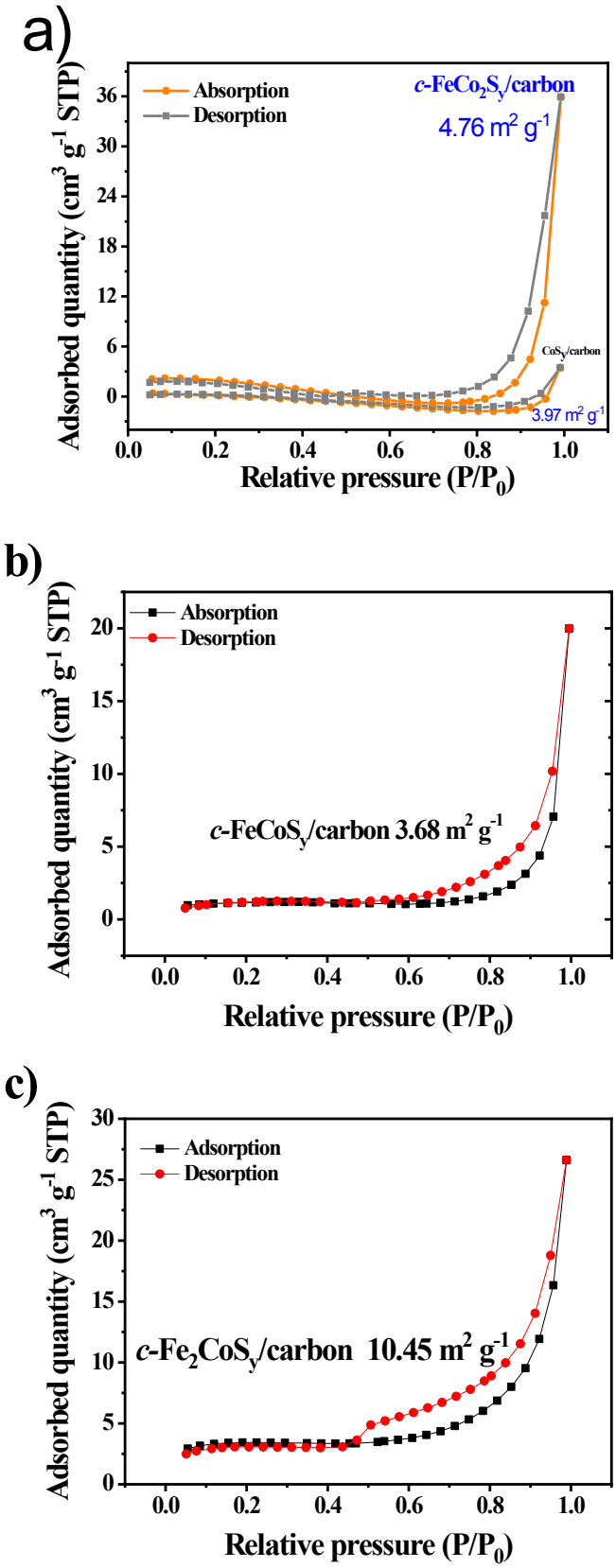

Figure SI-7. N_2 adsorption-desorption isotherms for a) CoS_y/carbon and *c*-$FeCo_2S_y$/carbon, b) *c*-$FeCoS_y$/carbon, c) *c*-Fe_2CoS_y/carbon.

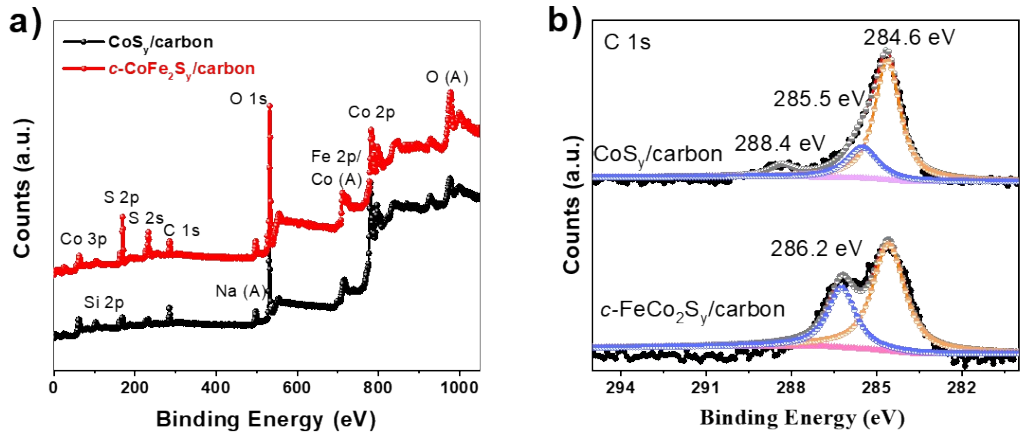

Figure SI-8. a) XPS survey and b) high-resulution C*1s* spectra of the CoS_y/carbon and *c*-$FeCo_2S_y$/carbon products. The XPS survey spectra suggesting the presence of Fe, Co, S, C, O elements in the products. The Si 2p band would come from the substrate to load the sample for XPS test. The presence of Na is due to the inevitable residue from Na_2SO_4 used for the synthesis.

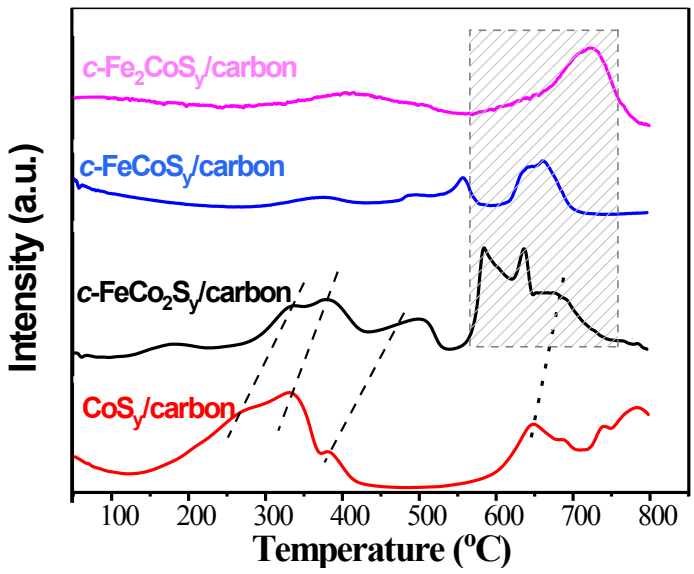

Figure SI-9. H_2-TPR spectra of CoS_y/carbon, *c*-$FeCo_2S_y$/carbon, *c*-$FeCoS_y$/carbon, *c*-Fe_2CoS_y/carbon products.

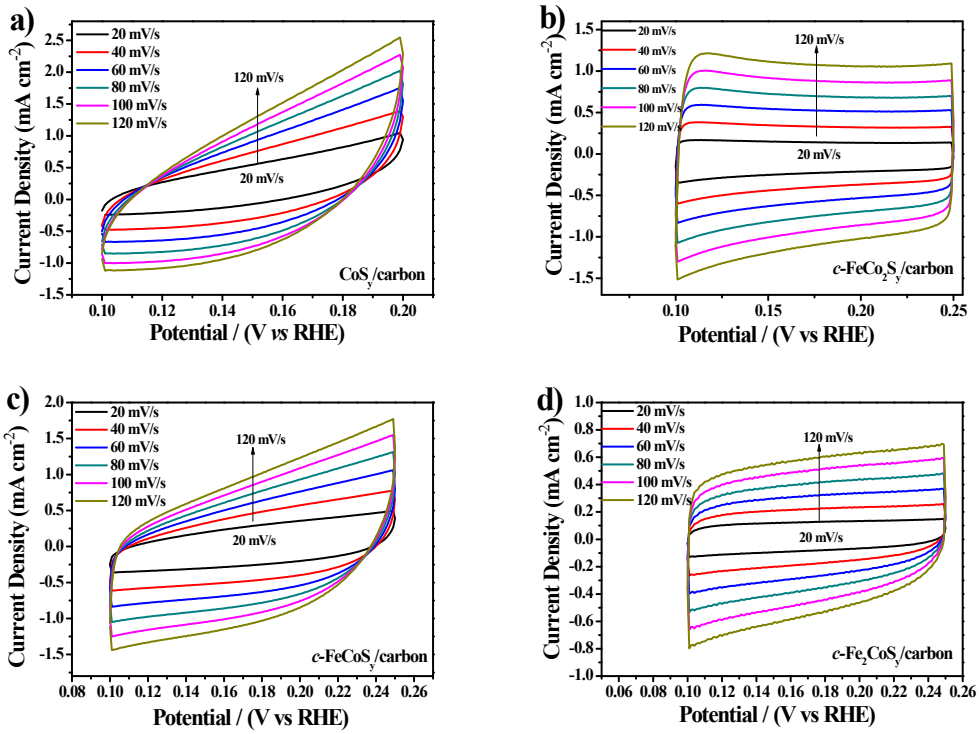

Figure SI-10. CV curves of the catalysts with different scanning rates. a) CoS_y/carbon, b) *c*-$FeCo_2S_y$/carbon, c) *c*-$FeCoS_y$/carbon, d) *c*-Fe_2CoS_y/carbon.

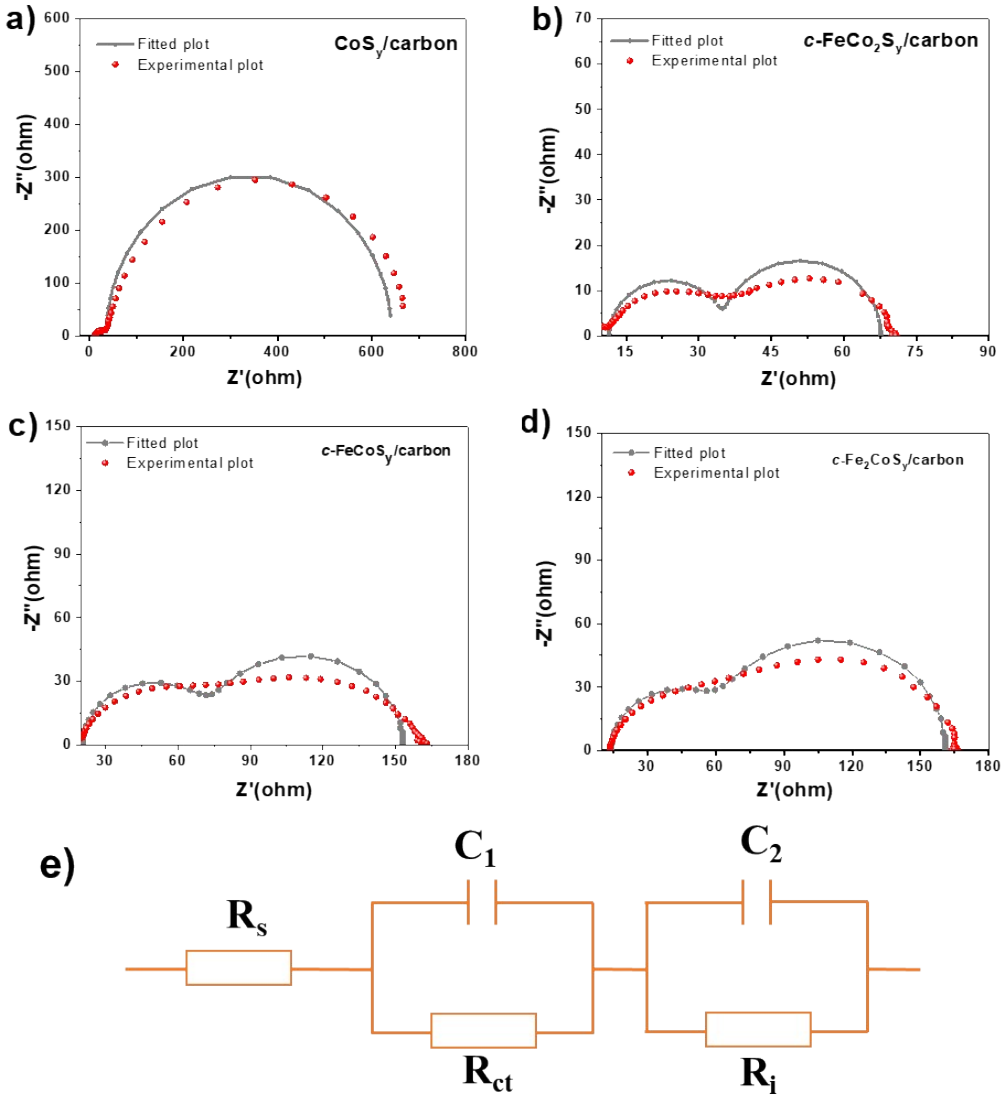

f)

Samples	R_s (ohm)	R_{ct} (ohm)	R_i (ohm)	C_1 (F)	C_2 (F)
CoS_y/carbon	12.3	606.2	24.0	1.7×10^{-4}	5.6×10^{-6}
c-Co_2FeS_y/carbon	11.5	32.7	23.6	2.8×10^{-4}	4.7×10^{-6}
c-$CoFeS_y$/carbon	14.5	38.3	31.8	1.7×10^{-4}	5.8×10^{-6}
c-$CoFe_2S_y$/carbon	16.7	81.6	48.1	1.0×10^{-4}	3.0×10^{-6}

Figure SI-11. Nyquist plots with fitted results from the equivalent RC circuit for the products of a) CoS_y/carbon, b) c-$FeCo_2S_y$/carbon, c) c-$FeCoS_y$/carbon, and d) c-Fe_2CoS_y/carbon. e) Equivalent RC circuit used to fit the plots. f) The fitted results with various resistance values.

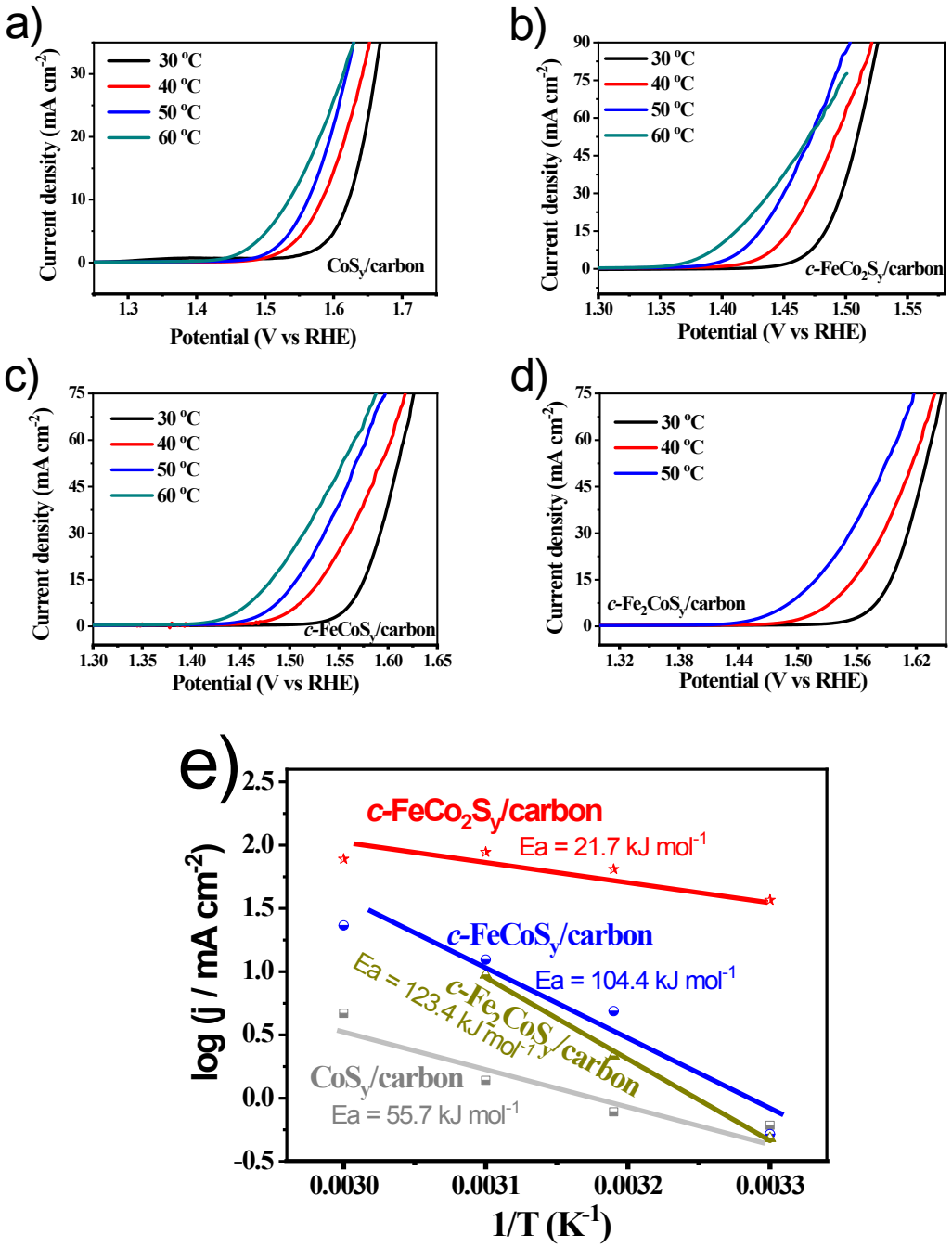

Figure SI-12. Polarization curves of the products for OER operated at different temperatures. a) CoS_y/carbon, b) *c*-$FeCo_2S_y$/carbon, c) *c*-$FeCoS_y$/carbon, d) *c*-Fe_2CoS_y/carbon. e) Arrhenius plots of the kinetic current at η = 270 mV without *iR* correction.

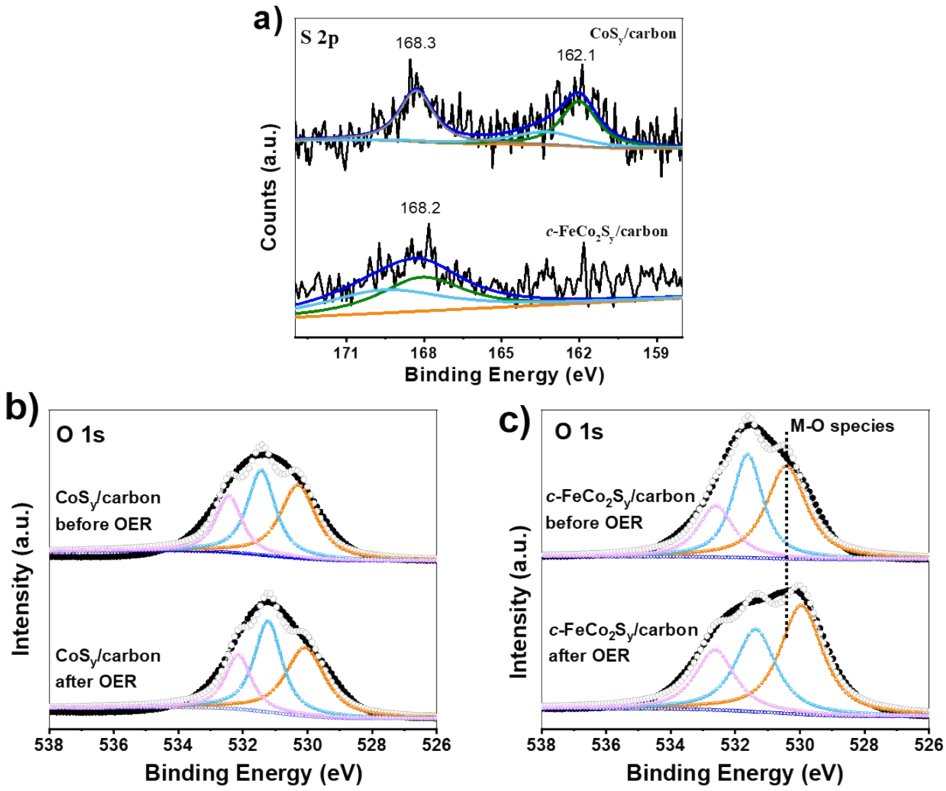

Figure SI-13. XPS spectra of a) S 2p region and b) O 1s region in the CoS_y/carbon and *c*-$FeCo_2S_y$/carbon products after OER test. For comparison, the O 1s spectra before OER tesing were also shown.

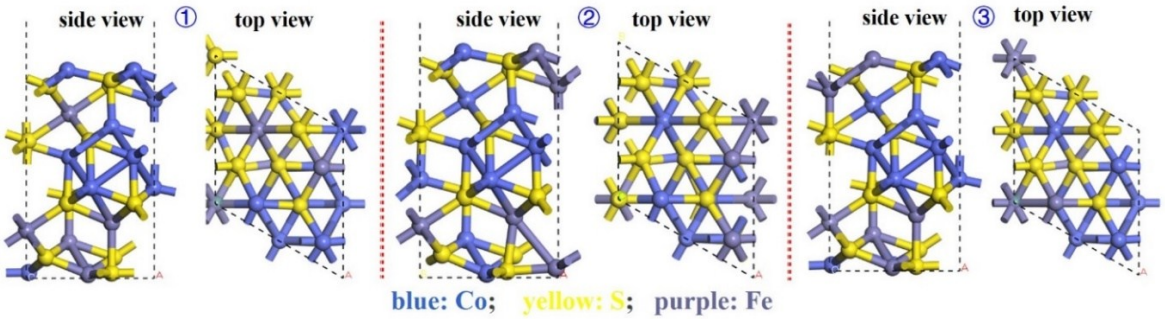

Figure SI-14. The top three most stable structures of $Fe_6Co_{12}S_{16}$ units (Blue, Co; yellow, S; purple, Fe).

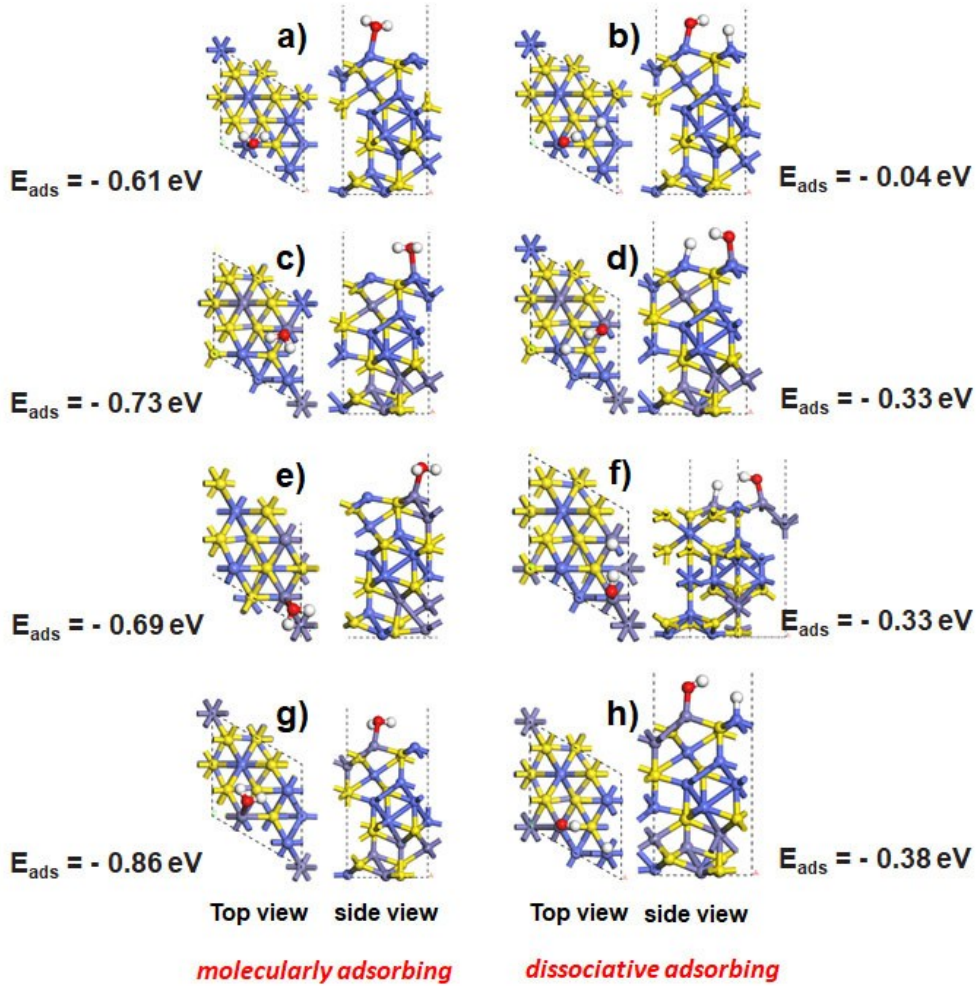

Figure SI-15. Optimized structure of water adsorbing model and the corresponding adsorbing energies (blue, Co sites; yellow, S sites; purple, Fe sites). Molecularly adsorbing on a) CoS_y, and c) structure ①, e) structure ②, g) structure ③ of $FeCo_2S_y$ clusters. Dissociative adsorbing on b) CoS_y, and d) structure ①, f) structure ②, h) structure ③ of $FeCo_2S_y$ clusters.

The possible configuration for water molecular adsorption on metal sulfides was then examined. For CoS_y, the result shows that in the most stable adsorption model, the water molecule inclines to adsorbing on a surface cobalt site through its O atom with an adsorption energy of -0.61 eV (Figure SI-15a). Our result also reveals that the water molecule prefers to molecularly adsorbing on the surface, rather than

dissociating into hydroxyl and H_{ad} (i.e., dissociative adsorption). The latter one presents an adsorption energy of only -0.04 eV (Figure SI-15b).

In contrast, when iron was introduced into the sulfide cluster, H_2O molecules are found to preferably interact with Fe sites by their O atoms (Figure SI-15). It is reasonable because the electron transfer effect between Fe and S sites induces lower electron density on iron. For example, the adsorption energy of H_2O on Fe sites of $Fe_6Co_{12}S_{16}$ clusters is -0.86 eV with the case of molecular adsorption mode (Figure SI-15) on structure ③ of $FeCo_2S_y$ clusters. The adsorption energy is much bigger than that of Co_9S_8 (-0.61 eV) and is also contrast to the adsorption energy (-0.58 eV) on the Co sites of $Fe_6Co_{12}S_{16}$ cluster. In the case of dissociative adsorption mode on $Fe_6Co_{12}S_{16}$ clusters (Figure SI-15h), a hydrogen atom is located on the interfacial Co site, with a hydroxyl staying on the iron sites. The corresponding adsorption energy is -0.38 eV, which are also bigger than that on Co_9S_8 (-0.04 eV) (Figure SI-15b). The above results indicate that on the sulfide surface, the molecular adsorption of water is more thermodynamically favorable than the dissociative adsorption on both of CoS_y and *c*-$FeCo_2S_y$ surface. In addition, these theoretical results indicate that the Fe sites would active for the following catalytic process. Theoretical analysis on another two stable $Fe_6Co_{12}S_{16}$ clusters also provides similar results (Figure SI-15).

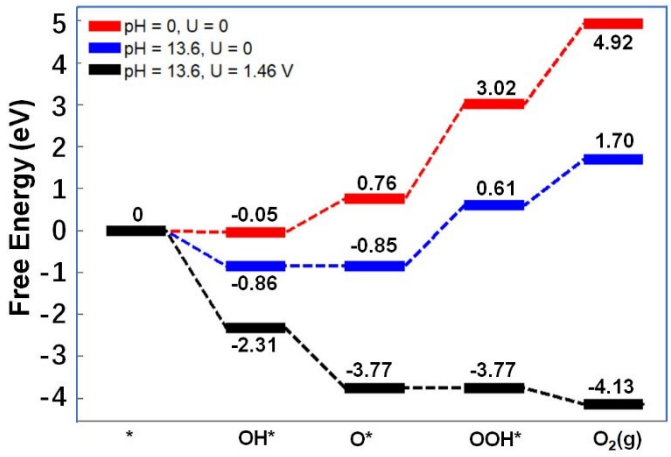

Figure SI-16. Full profile of Gibbs free energy for various intermediates in OER process. The theoretical overpotential for the process at pH = 13.6 can be estimated to be [0.61-(-0.85)]-1.23 = 0.23 V.

Table SI-1. Comparison studies of various typical FeCo-based OER electrocatalysts.

CoFe-based Materials	Electrolytes	Substrates	η (mV) for 10 mA cm^{-2}	Tafel slope (mV dec^{-1})	Stability	Refs.
$Co_{0.5}Fe_{0.5}S_x$/N-doped carbon	1 M KOH	GC	410	159	/	7
$Co_{0.37}Fe_{0.26}S$	1 M KOH	GC	270	37.2	27.4% current loss after 3 h	8
Fe-doped Co_9S_8	1 M KOH	Ni Foam	270	70	No current loss after 10 h	9
$Co_{0.5}Fe_{0.5}Se_2$	1 M KOH	Carbon fiber	290	64	Few current loss after 1000 cycles	10
$FeSe_2$@$CoSe_2$/rGO	1 M KOH	GC	260	36	Few current loss after 6 h	11
Co_7Fe-phyate	1 M KOH	GC	278	34	5.6% current loss after 10 h	12
$Co_{0.54}Fe_{0.46}P_x$ nanorods	0.1 M KOH	GC	370	/	No current loss after 1000 cycles	13
$CoFe_{1.7}P_x$	1 M KOH	GC	244	58	No current loss after 10 h	14
$Co_{0.4}Fe_{0.28}P$	1 M KOH	GC	270	26	No current loss after 3 h	8
Fe_3O_4/Co_3S_4 nanosheets	1 M KOH	GC	270	56	18% current loss after 24 h	15
Fe_3O_4/Co_9S_8/rGO	1 M KOH	GC	320	54	12% current loss after 6 h	16
Co_2FeO_x/rGO	1 M KOH	GC	340	~31	No increase of η after 4 h	17
Reduced $CoFe_2O_4$ nanosheets	1 M KOH	GC	320	48	9% current loss after 10 h	18
$Co_2Fe(OH)_x$	1 M KOH	Ni foam	300	83	20 mV increase of η after 20 h	19
$Co_3Fe(OH)_x$/rGO	0.1 M KOH	GC	325	43	No current loss after 10 h	20
c-$FeCo_2S_y$/carbon	1 M KOH	GC	247	35	No obvious current loss after 36 h	This work

Table SI-2. Bader charge analysis of the top three stable structures of $Fe_6Co_{12}S_{16}$ units (positive values mean electron density decrease; negative values mean electron density increase).

	structure ①	structure ②	structure ③	average
Fe	0.112	0.109	0.102	0.108
Co	-0.007	0.006	0.008	0.001
S	-0.105	-0.115	-0.110	-0.110

Table SI-3. Adsorption free energy of OH^- (ΔG_1) on the Co_9S_8 units and the top three stable structures of $Fe_6Co_{12}S_{16}$ units at different pH values.

Adsorption free energy of OH^- (ΔG_1) (eV)	Co_9S_8	Structure ①	Structure ②	Structure ③	Average value of structure ①②③
pH = 0 (ΔG_{H+}(pH) equals 0)	0.35	-0.16	0.14	-0.05	-0.023
pH = 13.6 (experimental conditions)	-0.45	-0.96	-0.66	-0.86	-0.827

Refernces:

1. M. Ramos, G. Berhault, D. A. Ferrer, B. Torres and R. R. Chianelli, *Catal. Sci. Techn.*, 2012, **2**, 164-178.
2. Y. P. Liu, Q. J. Li, R. Si, G. D. Li, W. Li, D. P. Liu, D. J. Wang, L. Sun, Y. Zhang and X. X. Zou, *Adv. Mater.*, 2017, **29**, 1606200.
3. J. Zhang, J. Liu, L. Xi, Y. Yu, N. Chen, S. Sun, W. Wang, K. M. Lange and B. Zhang, *J. Am. Chem. Soc.*, 2018, **140**, 3876-3879.
4. M. Bajdich, M. Garcia-Mota, A. Vojvodic, J. K. Norskov and A. T. Bell, *J. Am. Chem. Soc.*, 2013, **135**, 13521-13530.
5. Y. Mao, Z. Wang, H.-F. Wang and P. Hu, *ACS Catal.*, 2016, **6**, 7882-7891.
6. Z. Wang, X. M. Cao, J. Zhu and P. Hu, *J. Catal.*, 2014, **311**, 469-480.
7. M. X. Shen, C. P. Ruan, Y. Chen, C. H. Jiang, K. L. Ai and L. H. Lu, *ACS*

Appl. Mater. Interf., 2015, **7**, 1207-1218.

8. Z. Cao, T. Zhou, W. Xi and Y. Zhao, *Electrochim. Acta*, 2018, **263**, 576-584.
9. W.-K. Gao, J.-F. Qin, K. Wang, K.-L. Yan, Z.-Z. Liu, J.-H. Lin, Y.-M. Chai, C.-G. Liu and B. Dong, *Appl. Surf. Sci.*, 2018, **454**, 46-53.
10. J. Q. Chi, X. Shang, W. K. Gao, B. Dong, K. L. Yan, X. Li, Y. R. Liu, Y. M. Chai and C. G. Liu, *Int. J. Hydrogen Energ.*, 2017, **42**, 15189-15195.
11. G. Zhu, X. Xie, X. Li, Y. Liu, X. Shen, K. Xu and S. Chen, *ACS Appl. Mater. Interf.*, 2018, **10**, 19258-19270.
12. Y. J. Zhang, T. T. Gao, Z. Y. Jin, X. J. Chen and D. Xiao, *J. Mater. Chem. A*, 2016, **4**, 15888-15895.
13. A. Mendoza-Garcia, D. Su and S. H. Sun, *Nanoscale*, 2016, **8**, 3244-3247.
14. T. Zhang, J. Du, P. X. Xi and C. L. Xu, *ACS Appl. Mater. Interf.*, 2017, **9**, 362-370.
15. J. Du, T. Zhang, J. L. Xing and C. L. Xu, *J. Mater. Chem. A*, 2017, **5**, 9210-9216.
16. J. Yang, G. X. Zhu, Y. J. Liu, J. X. Xia, Z. Y. Ji, X. P. Shen and S. K. Wu, *Adv. Funct. Mater.*, 2016, **26**, 4712-4721.
17. J. Geng, L. Kuai, E. J. Kan, Q. Wang and B. Y. Geng, *ChemSusChem*, 2015, **8**, 659-664.
18. K.-L. Yan, X. Shang, Z.-Z. Liu, B. Dong, S.-S. Lu, J.-Q. Chi, W.-K. Gao, Y.-M. Chai and C.-G. Liu, *Int. J. Hydrogen Energ.*, 2017, **42**, 24150-24158.
19. L. X. Feng, A. R. Li, Y. X. Li, J. Liu, L. D. Y. Wang, L. Y. Huang, Y. Wang and X. B. Ge, *ChemPlusChem*, 2017, **82**, 483-488.
20. X. T. Han, C. Yu, J. Yang, C. T. Zhao, H. W. Huang, Z. B. Liu, P. M. Ajayan and J. S. Qiu, *Adv. Mater. Interf.*, 2016, **3**, 1500782.